The VMC survey[*]

III. Mass-loss rates and luminosities of LMC AGB stars

M. Gullieuszik[1], M. A. T. Groenewegen[1], M.-R. L. Cioni[2,3,**], R. de Grijs[4,5], J. Th. van Loon[6], L. Girardi[7], V. D. Ivanov[8], J. M. Oliveira[6], J. P. Emerson[9], and R. Guandalini[2]

[1] Royal Observatory of Belgium, Ringlaan 3, 1180 Brussel, Belgium
[2] University of Hertforshire, Physics Astronomy and Mathematics, Hatfield AL10 9AB, United Kingdom
[3] University Observatory Munich, Scheinerstrasse 1, 81679 München, Germany
[4] Kavli Institute for Astronomy and Astrophysics, Peking University, Yi He Yuan Lu 5, Hai Dian District, Beijing 100871, China
[5] Department of Astronomy and Space Science, Kyung Hee University, Yongin-shi, Kyungki-do 449-701, Republic of Korea
[6] Astrophysics Group, Lennard-Jones Laboratories, Keele University, Staffordshire ST5 5BG, UK
[7] INAF, Osservatorio Astronomico di Padova, Vicolo dellOsservatorio 5, 35122 Padova, Italy
[8] European Southern Observatory, Av. Alonso de Crdoba 3107, Casilla 19, Santiago, Chile
[9] Astronomy Unit, School of Physics & Astronomy, Queen Mary, University of London, Mile End Road, London, E1 4NS, UK,

ABSTRACT

Context. Asymptotic Giant Branch (AGB) stars are major contributors to both the chemical enrichment of the interstellar medium and the integrated light of galaxies. Despite its importance, the AGB is one of the least understood phases of stellar evolution. The main difficulties associated with detailed modelling of the AGB are related to the mass-loss process and the 3rd dredge-up efficiency

Aims. To provide direct measures of mass-loss rates and luminosities for a complete sample of AGB stars in the Large Magellanic Cloud, disentangling the C- and O-rich stellar populations.

Methods. Dust radiative transfer models are presented for all 374 AGB stars candidates in one of the fields observed by the new VISTA survey of the Magellanic Clouds (VMC). Mass-loss rates, luminosities and a classification of C- and O-rich stars are derived by fitting the models to the spectral energy distribution (SED) obtained by combining VMC data with existing optical, near-, and mid-infrared photometry.

Results. The classification technique is reliable at a level of – at worst – 75% and significantly better for the reddest dusty stars. We classified none of the stars with a relevant mass-loss rate as O-rich, and we can exclude the presence of more than one dusty O-rich star at a ∼ 94% level. The bolometric luminosity function we obtained is fully consistent with most of the literature data on the LMC and with the prediction of theoretical models, with a peak of the C-star distribution at $M_{bol} \simeq -4.8$ mag and no stars brighter than the classical AGB tip, at $M_{bol} = -7.1$ mag.

Conclusions. This exploratory study shows that our method provides reliable mass-loss rates, luminosities and chemical classifications for all AGB stars. These results offer already important constraints to AGB evolutionary models. Most of our conclusions, especially for the rarer dust-enshrouded extreme AGB stars, are however strongly limited by the relatively small area covered by our study. Forthcoming VMC observations will easily remove this limitation.

Key words. stars: AGB and post-AGB – stars: mass loss – Magellanic Clouds

1. Introduction

The Asymptotic Giant Branch (AGB) is the last stage of active nuclear burning for low and intermediate mass (∼0.8-8 $M_\odot$) stars. Although it is a short-lived phase – less than a few Myr (Girardi et al. 2010) – AGB stars are major polluters of the interstellar medium and major contributors to the integrated light of galaxies (Renzini & Buzzoni 1986). In spite of its relevance, the AGB is one of the least understood phases of stellar evolution, and a major source of disagreement between the results of different population synthesis models. This is mainly due to the difficulties associated with modelling convective dredge-up and mass-loss processes.

Most of the available sets of evolutionary tracks and isochrones cover AGB evolution in a very approximate way, ig-

noring crucial aspects of the AGB evolution. A more successful approach is based on synthetic codes, in which the stellar evolution is described by means of simplified relations derived from complete stellar models, while convective dredge-up and mass loss are tuned by means of a few adjustable parameters (Renzini & Voli 1981; Groenewegen & de Jong 1993; Marigo 2002; Cordier et al. 2007). This approach provided the first database of stellar isochrones suitable for reproduction of the basic observed properties of AGB stars, and in particular the bright red tail of carbon stars (Marigo et al. 2008). Despite the great success of these models, there are still some parameters (e.g., 3rd dredge-up and mass-loss efficiency) that need a detailed calibration, as shown by the disagreement between the observed number and luminosity function (LF) of C- and O-rich stars in nearby galaxies and model predictions (Gullieuszik et al. 2008; Held et al. 2010; Girardi et al. 2010). A more detailed calibration of the models requires measures of mass-loss rates and a

reliable classification of C-rich and O-rich AGB stellar populations in nearby stellar systems.

Direct measures of mass-loss rates in AGB stars are limited to samples of a hundred stars in the Magellanic Clouds (van Loon et al. 2008; Groenewegen et al. 2009). Estimates using larger samples of stars are, to date, based on empirical relations between mid-infrared (IR) colours and mass-loss rates (Matsuura et al. 2009). Recently, Srinivasan et al. (2009) used mid-IR photometry from the SAGE survey (Meixner et al. 2006) to identify thousands of AGB star candidates in the LMC. Their spectral energy distributions (SED) were fitted with dust-free photospheric models for O- and C-rich stars. The mass-loss rates were then derived from the excess in the fluxes observed in the 8 and 24 μm bands. This was the first step of an ongoing project aimed at directly measuring mass-loss rates for all their candidates using a grid of dust shell models (see Sargent et al. 2011).

To calibrate the 3rd dredge-up efficiency complete catalogues of O- and C-rich AGB stars are needed. The most straightforward method to obtain a reliable classification uses a spectroscopic classification, but this would be extremely expensive in terms of observing time. The most recent and impressive effort in this direction is the SAGE-Spec (Woods et al. 2011) spectroscopic survey, which aims at a classification of mid-IR sources (mainly AGB stars) in the LMC. The project was awarded 224.6 hr of Spitzer Space Telescope observations, and provided a reliable classification of 197 point sources. This is clearly a minor fraction of the total LMC AGB population, which consists of some tens of thousands of stars (Cioni et al. 2006). A more efficient, although in principle less reliable way to achieve a classification employs photometric data. Different approaches have been adopted, mainly involving either optical narrow-band or near-IR broad-band photometry (e.g., Battinelli & Demers 2005; Gullieuszik et al. 2008; Held et al. 2010).

The Magellanic Clouds (MC) are ideal targets to study the details of AGB evolution, since they host a huge population of AGB stars covering the whole age (i.e. initial mass) range and they are nearby galaxies, easily accessible for observations of resolved stellar populations. The immediate drawback of the proximity is the large sky area covered by the MCs. Only recently have some observational campaigns provided coverage of a significant fraction of both the LMC and the SMC, in particular: the optical Magellanic Clouds Photometric Survey (MCPS, Zaritsky et al. 2002, 2004); the all-sky 2MASS (Skrutskie et al. 2006) and the MCs IRSF (Kato et al. 2007) surveys in the near-IR; the SAGE-LMC (Meixner et al. 2006), SAGE-SMC (Gordon et al. 2011), S^{3}MC (Bolatto et al. 2007) Spiter surveys, and the AKARI/IRC LMC survey (Ita et al. 2008) in the mid-IR.

The VISTA Magellanic Cloud survey (VMC, Cioni et al. 2011) is one of the six ESO public survey projects that are carried out with the new ESO telescope VISTA (Emerson & Sutherland 2010). It aims at imaging about 180 square degrees in the Magellanic system (LMC, SMC, the Bridge and the Stream) in the YJK_s wavebands, reaching a depth of $K_s \sim 20.5$ mag, nearly 5 mag deeper than 2MASS and $\sim$ 3 mag deeper than IRSF. Observations started in November 2009 and will take about five years to reach completion. The first images and catalogues were released to the community in 2011 and new data will be released at regular intervals according to the ESO policy for public surveys. The VMC data will provide, e.g., a detailed history of star formation across the Magellanic system and a measurement of its 3D geometry. The VMC is described in more detail in Cioni et al. (2011); a series of papers will present the scientific results of the survey. To date, Miszalski et al. (2011) presented a multi-wavelength study of

LMC planetary nebulae and Rubele et al. (2011) obtained a spatially resolved Star Formation History of the LMC fields already observed by the VMC.

We aim at extending the direct measure of luminosity and mass-loss rate to the whole AGB stellar population in the Magellanic system by modelling the SEDs obtained by collecting all available photometry from optical to mid-IR wavelengths. VMC observations are particularly important, because their photometric quality and spatial resolution are much higher than that of 2MASS. This yields a more accurate photometry, in particular for the extremely red dust enshrouded AGB stars, around the detection limit of 2MASS in the bluest bands – $J \sim 16.5$ mag and $K_s \sim 15.0$ mag. In addition AGB stars are variables and the addition of VMC data –taken at a different epoch from e.g. 2MASS– will result in a more robust estimate of the mean luminosity and mass-loss rate of the star. The SED analysis also provides a classification of the stellar chemical composition. To test its power to disentangle O- and C-rich AGB stellar populations, we present a critical comparison between our results and spectroscopic classifications from the literature.

In this paper we present our first results, based on data of the LMC region covered by the first VMC observations. The data and the AGB selection criteria are presented in Sect. 2; Section 3 describes our model; the results are presented in Sect. 4; in Sect. 5 we summarise our work.

2. The data

We used the v1.0 VMC release, which is described in detail in Cioni et al. (2011). The data were processed by the VISTA Data Flow System (Emerson et al. 2004) pipeline (Irwin et al. 2004) and retrieved from the VISTA Science Archive (Hambly et al. 2004). The major issue for AGB stars in VMC photometry is saturation and non-linearity of the detectors for bright objects. The VISTA pipeline provides a correction for saturation effects which can recover reliable photometry for stars up to $\sim$ 2 mag brighter than the saturation limit. This is however not enough, since some AGB stars are even brighter, so we had to reject VMC photometry for stars brighter than 10.5 mag in the Y and J bands and 10.0 mag in the K_s band (see Cioni et al. 2011).

Additional photometry was obtained by collecting data from LMC photometric surveys:

– optical: $UBVI$ data from the MCPS (Zaritsky et al. 2004);
– near-IR: JHK_s data from the all-sky 2MASS (Skrutskie et al. 2006), and the extended mission 6x long-exposure release; stars with very poor photometry – quality flag "E" – in any of the JHK_s bands were discarded;
– mid-IR: IRAC 3.6, 4.5, 5.8, 8.0 and MIPS 24, 70, 160 μm data from the SAGE catalogue (Meixner et al. 2006); we used the `SAGELMCcatalogIRAC` and `SAGEcatalogMIPS24` catalogues containing both SAGE epochs 1 and 2 separately to avoid losing information on variability;
– mid-IR 9 and 18 μm photometry from the AKARI/IRC mid-infrared all-sky survey (Ishihara et al. 2010).

The SED of each star was obtained using all photometric data points. When a single magnitude for each photometric band was needed, e.g., to plot colour-magnitude diagrams (CMDs), the data were merged. For mid-IR photometry we used the original SAGE epoch-merged data, while VMC and 2MASS J and K_s were averaged after applying the colour equations to transform J and K_s 2MASS photometry to the VISTA photometric system (Cioni et al. 2011).

For our project the use of optical and mid-IR photometry is fundamental, so we will limit our analysis to the areas of the MCs observed by all of the VMC, the MCPS and Spitzer. To date, there are only two VMC fields in common with the optical and mid-IR surveys, namely fields 6_6 and 8_3 (see Cioni et al. 2011). The first is centred on the 30 Doradus star-forming region, which is affected by severe crowding and differential reddening problems. Since in this paper we want to define our methodology and test its reliability, it is clear that data obtained from observations of field 6_6 are not a suitable benchmark. We consequently base the analysis presented in this paper on data in VMC field 8_3, and in particular in the 1.42 deg^2 region delineated by $75°\!.50 < \alpha(\text{J2000}) < 77°\!.50$ and $-66°\!.95 < \delta(\text{J2000}) < -65°\!.19$.

The targets for our analysis were selected using near- and mid-IR photometry. We used 2MASS magnitude for selection rather than VMC ones, since some bright AGB stars have no reliable VMC photometry because of saturation.

The only problem with this choice could be those AGB stars that are heavily obscured by thick circumstellar dusty discs with extremely red colours that are too faint in the near-IR for detection by 2MASS. We verified this hypothesis and checked that no such sources exist in the current sample. The conditions we imposed are:

- $J - K_s > -0.075 \times K_s + 1.85$, the relation defined by Cioni et al. (2006) to minimise contamination by foreground Milky Way and LMC red supergiant stellar populations.
- K_s brighter than 12.0 mag, which corresponds to the tip of the RGB (TRGB) (Cioni et al. 2000). This condition was applied only to stars with $J - K_s < 1.5$ mag, since redder stars cannot be RGB stars, and extremely red dust enshrouded AGB stars can be fainter than the K_s-band TRGB.
- IRAC 4.5 μm magnitude brighter than 12.0 mag. This condition was set to avoid sources with faint mid-IR emission which cannot be AGB stars, but may be rather artifacts in the 2MASS catalogue.

These criteria define a sample of 372 candidate AGB stars. We note that only 15 of them have 9 μm AKARI photometry and only 4 are detected in the 18 μm AKARI band. None are present in the AKARI/FIS All-Sky Survey Bright Source Catalogue. Finally, only one of the selected sources was detected in the MIPS 160 μm band and three at 70 μm. All of these objects turned out to have SEDs that are incompatible with AGB stars (see next section).

The selection criteria defined above could in principle exclude the most extremely red AGB stars, like those discovered by Gruendl et al. (2008) using mid-IR photometry and spectroscopy. Their SEDs peak in the mid-IR at wavelengths $\gtrsim 10\,\mu$m and they are extremely faint in bluer wave-bands. Some of the stars in Gruendl et al. (2008) sample have IRAC 4.5 μm magnitudes fainter than 12.0 mag, and they could be likely fainter than the VMC detection limit. For this reason, we added an additional selection criterion, based on mid-IR photometry, to include extremely red stars in our sample. Using all the stars classified as candidate AGB stars by Gruendl & Chu (2009), we defined the following selection rules: $[4.5]-[8.0] > 1$ and $[8.0] < 8.5 + 0.25 \times ([4.5] - [8.0])$, which correspond to the box displayed in the lower-right panel of Fig. 1. This criterion adds two objects to our sample. Anticipating the results that will be presented in the next sections, we can safely exclude that the bluest of the two objects is an AGB star. The classification of second one is quite unclear, but in the Appendix of this paper we

provide some evidence that also this object could not be an AGB star.

3. The model

We fitted the SEDs with a combination of photospheric models, dust models and by solving the radiative transfer equation. The code used in this paper is based on that presented by Groenewegen et al. (2009), updated to use the DUSTY code (Ivezić et al. 1999) to solve the radiative transfer equation (Groenewegen, in prep.). Another important update is the use of Aringer et al. (2009) models for the stellar atmosphere of C-rich stars. For O-rich stars MARCS models (Gustafsson et al. 2008) were used.

We adopted only two different dust-grain compositions, following Groenewegen et al. (2009). A 94% amorphous carbon + 6% SiC mixture was assumed for C-rich stars, and "astronomical silicates" with the absorption coefficients of Volk & Kwok (1988) for O-rich stars. Since we are considering only broadband photometry, we preferred to apply the results of Groenewegen et al. (2009), based on mid-IR spectroscopy, rather than introducing the dust composition as a free parameter weakly constrained by the data used in our analysis.

The observed SED is fitted using a minimisation technique to find the best-fitting values for the luminosity and optical depth τ_λ at 0.55 μm of the dusty shell under the assumption of a r^{-2} density profile. The minimisation is based on reduced χ^2 ($\chi^2_{\rm r}$), which was calculated by taking into account the photometric errors. The mass-loss rate $\dot{M}$ was computed using the relation of Groenewegen et al. (1998), applied to a geometrically thick shell, since we assumed an outer to inner radius ratio of 10^4 (Groenewegen et al. 2009):

$$\tau_\lambda = 5.405 \times 10^8 \frac{\dot{M}\,\Psi\,Q_\lambda/a}{r_{\rm d}\,R_\star\,v_{\rm exp}\,\rho_{\rm d}}, \tag{1}$$

where $\dot{M}$ is in $M_\odot$ yr^{-1}, $v_{\rm exp}$ is the shell expansion velocity in km s^{-1}, $R_\star$ is the stellar radius in solar radii, $r_{\rm d}$ is the inner dust radius in stellar radii, Q_λ is the absorption coefficient, a is the dust grain radius in cm, Ψ is the dust-to-gas mass ratio, and $\rho_{\rm d}$ is the grain density in g cm^{-3}. The values of Q_λ/a and $R_\star$ were obtained from the dust and stellar models, respectively, while $r_{\rm d}$ is an output of the dust radiative code. We adopted $v_{\rm exp} = 10$ km s^{-1} and $\Psi = 0.005$. These are standard values for AGB stars in our Galaxy, which may not apply to the most metal-poor stars in the LMC (see, e.g., van Loon et al. 2008).

The sample of stars was divided into a "Red" and a "Blue" group, using as a discriminant the condition $J - K_s > 1.5$ mag. The number of stars in the red and blue groups is 97 and 274, respectively. The first group consists of the so-called red tail, the location in the CMD where most of the mass-losing C-stars are found. With this choice, in the "Red" group there are mostly low effective temperature dusty stars, whose SEDs are dominated by dust emission. In this case the choice of the atmospheric model is therefore not critical. On the other hand, bluer stars are expected to have higher $T_{\rm eff}$ and lower mass-loss rates and their SEDs are determined largely by the stellar photosphere rather than the dust envelope, making the choice of photospheric model more critical. For the stars in this group we used a wider temperature range. Since the bluest stars are expected to have very low to negligible mass-loss rates, for all temperatures we considered the possibility of having dust-free models, fixing the mass-loss rate at zero. Only for the two lowest temperatures we left the
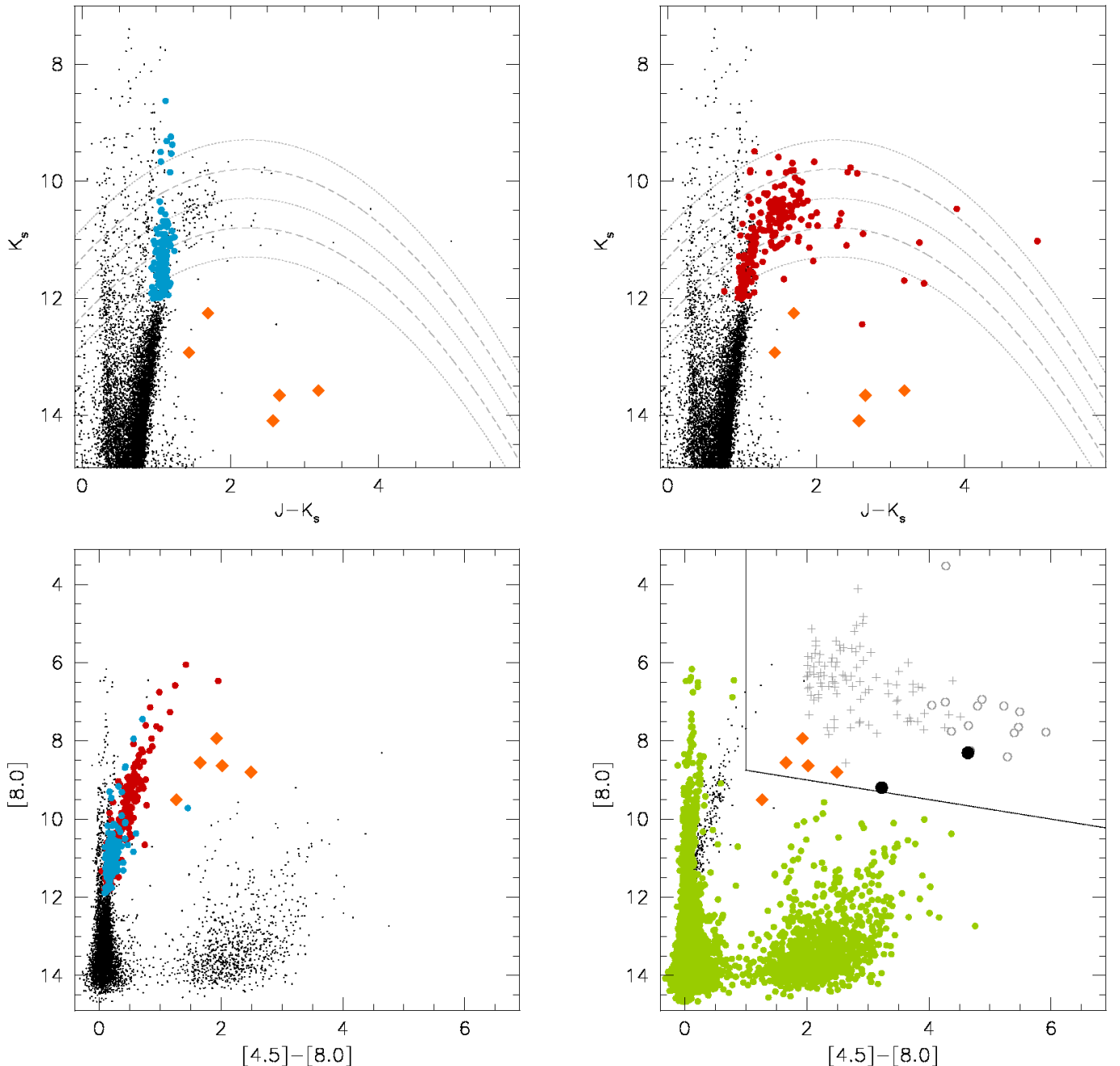
Fig. 1: Near- (*upper panels*) and mid-IR (*lower panels*) CMDs for stars in the VMC field 8_3. Stars classified as O-rich (*upper left panel, blue dots*) and C-rich (*upper right panel, red dots*) are shown as solid symbols. The five non-AGB sources are displayed as diamonds. In the upper panels we plotted curves of constant bolometric magnitudes (M_{bol} between -6.0 and -4.0, with steps of 0.5 mag) derived using the K_s-band bolometric correction from Kerschbaum et al. (2010). In the lower-left panel all AGB stars are shown as bigger points, while in the lower-right panel bigger (green) points show all stars not classified as AGB candidates using the near-IR criteria. The small grey crosses and open circles show all the sources in the LMC classified as AGB stars and EROs, respectively, by Gruendl & Chu (2009). The filled circles represent the two additional stars selected purely on the basis of the mid-IR photometry using the area delineated by the solid line.

mass-loss rate as a free parameter. These considerations lead to the definition of the adopted grid of atmospheric models, summarised in Table 1. For the dusty models, we considered four different values for the condensation temperature of the dust grains ($T_c = 800, 900, 1000,$ and 1200 K). In conclusion, for both groups we ran a set of 24 models; for the "Red" group we have 13 C-rich (two with four different T_c plus five dust-free)

and 11 O-rich (two with four different T_c plus three dust-free) models; for the "Blue" group we have 12 (three with four different T_c) C-rich and 12 O-rich models. For all stars we adopted a distance of 50 kpc (e.g., Schaefer 2008), an extinction $A_V = 0.25$ mag (Schlegel et al. 1998), and the Cardelli et al. (1989) extinction law.

Table 1: The model grid. For each group ("Blue" and "Red") and chemical composition, we list the temperatures adopted for models with the mass-loss rate set at zero ("0") or as a free parameter ("F").

T_{eff} [K]	Blue				Red	
	C-rich		O-rich		C-rich	O-rich
2600	0	F			F	
2800					F	F
3000	0	F			F	
3200	0		0	F		F
3600	0		0	F		F
4000	0		0			

The model that yields the minimum χ_{r}^2 was taken as best-fitting solution. Figure 2 shows – as an example – the data and the best-fitting models for three stars. The complete list of figures with the SEDs and the best-fitting models for all stars are available as online material, while the χ_{r}^2 values are listed in Table 6. The parameters of best-fit models are presented in Table 2. All stars with a χ_{r}^2 higher than 300 have been flagged as *B* ("Bad fits"). Most (e.g., the reddest star in Fig. 2) are extremely red stars, i.e. high-amplitude long-period variables. The high χ_{r}^2 value can then be understood considering that our data are obtained from observations carried out at different epochs. Seven sources however have SEDs incompatible with AGB stars and they were therefore excluded from our analysis. Four (IDs 73, 130, and 133 and 165 in Table 2) are classified as candidate young stellar objects (YSO) (Woods et al. 2011; Gruendl & Chu 2009), one (ID 43) is a Seyfert galaxy at $z = 0.064$ (Véron-Cetty & Véron 2010), one (ID 14) is a post-AGB star (Woods et al. 2011). The last object (ID 75), is the source J050343.02-664456.7 in Gruendl & Chu (2009) which is generically classified as an Extremely Red Object (ERO). This is one of the two objects not detected by VMC which were included in our sample using the mid-IR selection criteria. The classification of this source is doubtful. Gruendl et al. (2008) argued it is an AGB star, but in the Appendix we show that its near-IR emission is unlikely to match the SED expected for an AGB star. We suggest that it may be a transition object, which left the AGB phase ~ 100 years ago, and entered post-AGB phase. Thus we excluded this star from our sample. The final sample of objects with SED compatible with AGB stars is therefore 367. The photometry for all of them is given in Table 6, available as online material.

The photospheric model of the best-fitting solution gives also a useful indication for classification of the stellar atmosphere as C- or O-rich. To estimate the confidence level of this classification, we calculated the relative difference between the two χ_{r}^2 values of the two best-fitting solutions obtained considering O- and C-rich models separately. A small difference indicates that the solutions obtained with C- and O-rich models are equally acceptable; if the difference is large, the solution with the lowest χ_{r}^2 gives a noticeably better description of the data, and in this case the classification has a higher confidence level. After some tests, a value of $\delta\chi_{\text{r}}^2 = \Delta\chi_{\text{r}}^2/\chi_{\text{r}}^2 = 1$ was adopted as discriminant. Stars with $\delta\chi_{\text{r}}^2 < 1$ were flagged as *uncertain*. Two tests as to the reliability of our classification – based on spectroscopic data from the literature– are provided in Sect. 4.1.

To check for any systematic effect in our modelling, Figs. 3 and 4 show the differences between the observed magnitudes and those calculated from the best-fitting model in each photo-

Table 2: Parameters of best-fitting models for all sources in our database. Only the first entries are shown here as an example. The full table is available at the CDS. The fourth column is the optical depth at 0.55 μm. For stars without a dusty envelope, the logarithm of the mass-loss rate (5th column), was set to -99.999. The 7th column indicates the C- and O-rich classification. Sources flagged "B" indicate stars with bad fits while "U" stands for uncertain classification and "S" for secure classification.

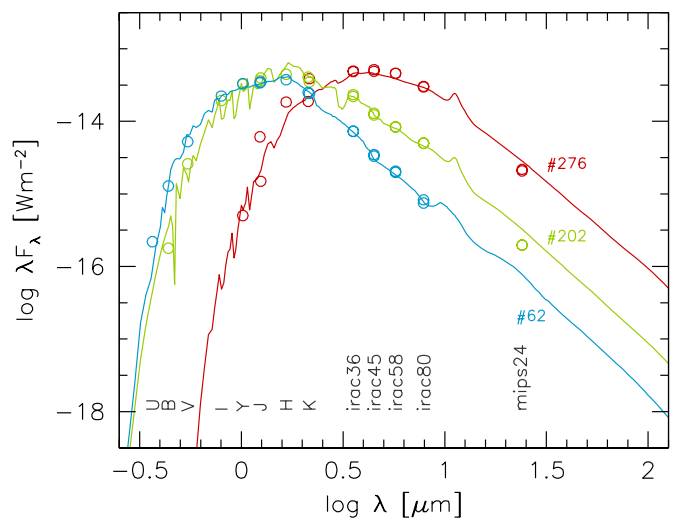| id	RA (J2000)	DEC (J2000)	$\tau_{0.55}$	$\log \dot{M}/M_{\odot}$	$L/L_{\odot}$	class	flag
1	05:02:00.86	−65:23:12.3	0.000	-99.999	3263	O	U
2	05:02:01.65	−66:16:00.2	0.000	-99.999	4847	O	U
3	05:02:02.88	−66:46:51.6	0.137	-7.462	5645	C	S
4	05:02:07.10	−66:56:03.1	0.019	-8.596	5402	O	S
5	05:02:09.01	−66:18:57.2	0.340	-7.069	5544	C	S

Fig. 2: Photometric data points (*open circles*) and the fitted SEDs (*lines*) for three AGB stars: a blue O-rich star ($J - K_s = 1.2$ mag, id 62), and two C-rich stars ($J - K_s = 1.5$ mag, id 202; and $J - K_s \sim 4$ mag, id 276).

metric band. The variations of the distributions' spreads can be explained considering that AGB stars are variable sources, with amplitudes that are higher for redder stars and in the bluer optical bands. At the bluest wavelengths (*B* and *V*), the variation amplitude is maximum, as is the photometric error, since all stars – especially those in the red sample – are faint (many red stars are not detected in the *B* band). On the other side of the spectrum, due to the limited sensitivity of the Spitzer Space Telescope in the reddest bands, most of the bluest stars are at the detection limit (only 45 out of the total of 274 blue stars are detected in the MIPS 24 μm band). The distribution of the residuals indicates a good quality of the fit for the stars in the blue sample, considering the photometric errors and the intrinsic variability of AGB stars. The residual distributions are in general broader for stars in the red sample; this is not surprising, since these are the stars with the highest amplitude variability, where the effects of the circumstellar dust are more significant. The scatter in the near-IR regime is similar in the red and in the blue samples, showing that the dust model – which mostly affects the SEDs of the red stars – is satisfactory. Figure 4 shows that there are systematic
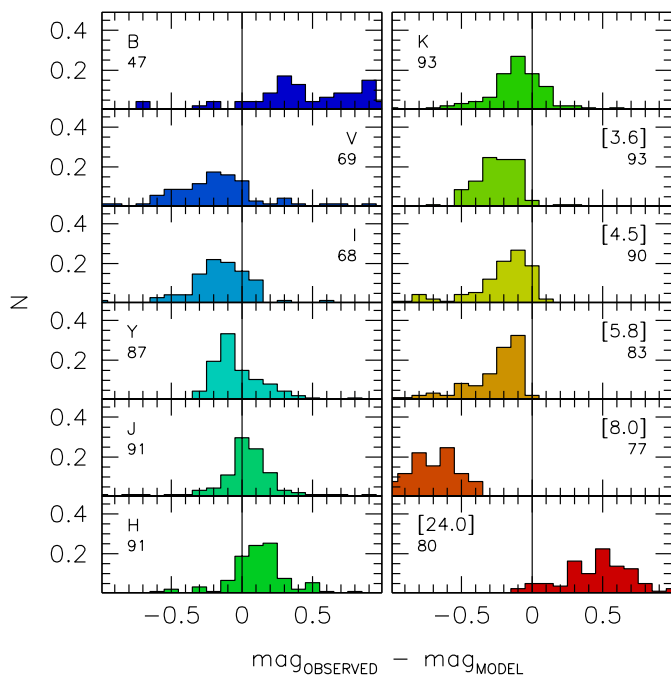
Fig. 4: Same as Fig. 3, but for stars with $J - K_s > 1.5$ mag.

Table 3: Results of the comparison with the classification by Groenewegen et al. (2009) and Groenewegen (in prep.). Numbers in parentheses refer only to stars with robust classification (see text).

	Blue		Red	
	C	O	C	O
total	46	72	113	29
	(38)	(44)	(93)	(22)
correct	93%	72%	97%	76%
	(95%)	(82%)	(100%)	(73%)

Table 4: Classification of AGB stars in the VMC 8_3 field.

	Blue		Red		All	
	C	O	C	O	C	O
Total	113	161	93	0	206	161
certain classification	54	93	78	0	132	93
uncertain classification	58	67	10	0	68	67
bad fit	1	1	5	0	6	1

offsets in the reddest magnitudes. Models are always too faint in the IRAC 8 μm and too bright in the MIPS 24 μm bands (see also Fig. 2). This effect is negligible for stars in the blue sample (Fig. 3). The geometry of the dust shell, as well as the size and chemical composition of dust grains, influence the details of the dust emission, and different combinations of these parameters could in principle produce SEDs with different slopes at the red end. The systematic offsets in our models are however not completely surprising, since a similar effect can be seen also in Groenewegen et al. (2009). They used a similar SED fitting technique, but with the addition of Spitzer spectra, giving fundamental information on the dust emission features. They could therefore obtain much more information about the dust properties. In this paper we assumed the dust properties that provided the best description of the dust emission.

4. Results

4.1. Reliability of the classification

To test the reliability of our C-/O-rich classification, we conducted two different tests. First, we considered the catalogue of C-stars in the LMC spectroscopically classified by Kontizas et al. (2001). We found 87 stars in common with their sample and all are relatively blue ($J - K_s \lesssim 2$ mag). Our procedure correctly classified as C-stars 87% of these. If we exclude the 20 stars with uncertain classification, this fraction increases to 96%. All 54 stars with ($J - K_s > 1.5$ mag) were correctly classified, while the success rate for the 33 bluer ($J - K_s \leq 1.5$ mag) stars is 67%, or 84% excluding the 14 stars with uncertain classification.

Second, we considered the stars in the catalogue of Groenewegen et al. (2009), complemented with other LMC and SMC AGB stars with Spitzer IRS mid-IR spectra (Groenewegen, in prep.[1]). The catalogue consists in 260 stars, and none of them

is located in VMC field 8_3. The photometric data were therefore taken from Groenewegen et al. For homogeneity with our analysis, only data in optical, 2MASS and Spitzer photometric bands were considered. We applied to the final catalogue of 260 stars our fitting procedure and compared our classification with that derived by Groenewegen et al. (2009, in prep.). The results are summarised in Table 3. The reliability of our classification is confirmed to be extremely high for C-stars. In this case we obtained a 95% confidence level for classification of Blue C-rich stars, which is slightly higher than the value obtained from the previous test based on the Kontizas et al. (2001) results, but fully consistent with it considering the low number of stars in the samples used for the two tests. For O-rich stars the confidence level is around 75%, similar as for red stars.

As an additional test, we considered the seven objects in the SAGE-Spec sample (Woods et al. 2011) located in the region used for our study. Although this number is extremely small, the spectroscopic SAGE-Spec classification is in perfect agreement with our results. One of them is one of the YSOs and another one is the post-AGB star already discussed. Three sources are red supergiants rightly excluded by the colour selection. Finally two sources are classified as C-AGB stars both by Woods et al. (2011) and by us.

4.2. C- and O- rich stellar populations

The results of our classification of the 367 AGB stars in VMC field 8_3 are summarised in Table 4 and in the two upper panels of Fig. 1. The location of C- and O-rich stars in the CMD agrees with predictions of AGB stellar models (e.g., see Fig. 7 in Marigo et al. 2008): O-rich stars with no –or small– dusty envelopes are located on a nearly vertical blue plume, while C-rich stars populate the reddest part of the CMD. In Marigo et al.

---

[1] Compared to Groenewegen et al. (2009), AGB and RSG stars from the following IRS programs were added: 30788 (PI: Sahai ,

no dedicated publication, 3 spectra are discussed in Buchanan et al. 2009); 40159 (PI: Kemper, the SAGE-SPEC program described in Kemper et al. 2010); 40650 (PI: Looney, see Gruendl et al. 2008); 50167 (PI: Clayton, no publication); 50240 (PI: Sloan, the SMC-SPEC program, see Sloan et al. 2010).
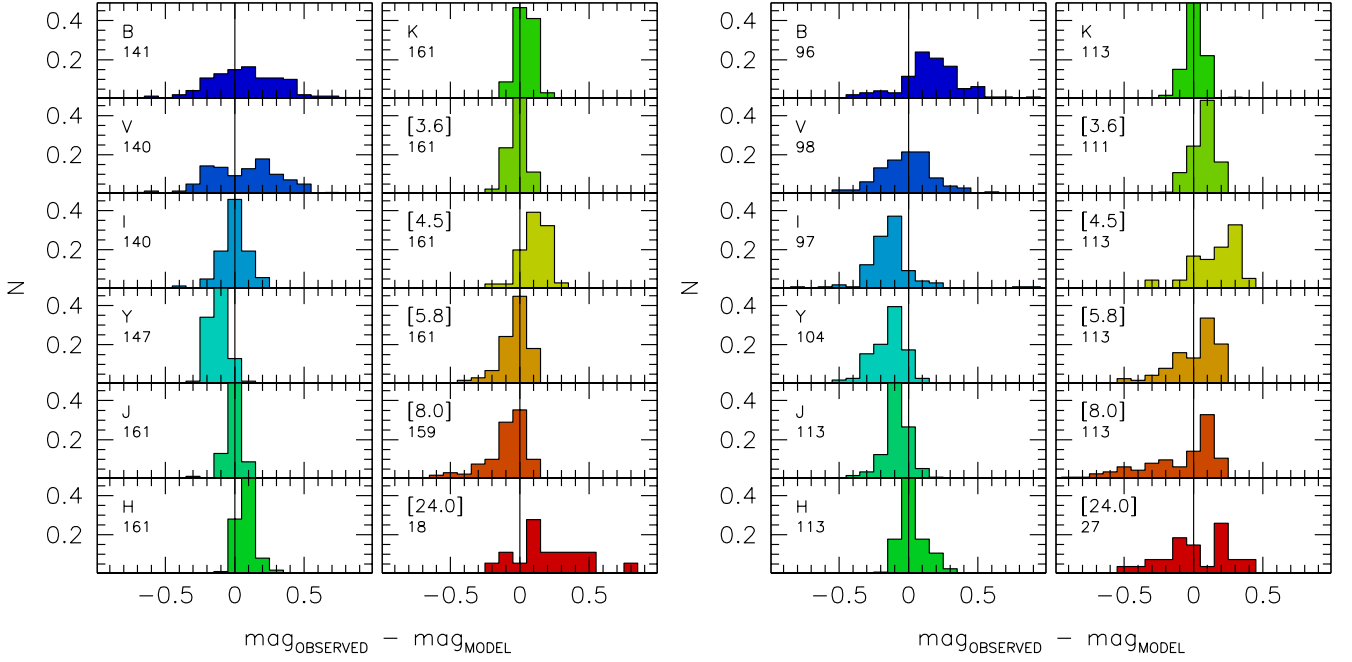
Fig. 3: Histograms of magnitude residuals for the data in all wave-bands, for O-rich (*left panel*) and C-rich (*right panel*) stars with $J - K_s < 1.5$ mag. The histograms are normalised to the total number of stars detected in each wave-band, labelled in each plot.

(2008) this is ascribed to the cool T_{eff} caused by changes in molecular opacities as the third dredge-up events increase the photospheric C/O ratio.

The most remarkable fact is that all red stars are found to be C-stars. We cannot exclude, in principle, that some of them could be misclassified O-rich. The results of our tests presented in Sect. 4.1 showed that the probability of an incorrect classification is around 25%. The presence of more than one O-rich dust-enshrouded star can therefore be excluded at a $\sim 94\%$ confidence level.

A very small number – if any – of red O-rich stars was expected a priori since dust-enshrouded O-rich stars are rare: low mass O-rich AGB stars do not reach high-mass rate (> $10^{-5} M_\odot \, \mathrm{yr}^{-1}$). On the other hand, the most massive O-rich AGB stars are intrinsically rare objects, because of the shape of the stellar initial mass function, which is dominated by low-mass stars in a power-law fashion. Dusty O-rich stars are therefore expected to be found preferentially in regions with a high star-formation rate at recent epochs (< 1 Gyr). The VMC 8_3 field, used for this preliminary study, is located in the outer regions of the LMC, where the recent star-formation rate is not particularly high (Rubele et al. 2011).

All the brightest stars in the blue vertical plume at $K_s < 10$ mag are classified as O-rich, as expected Marigo et al. (2008). That region of the CMD is in fact populated by the massive O-rich AGB stars in the hot bottom burning phase. However note that we cannot exclude that some of them could in principle be core He-burning red supergiants.

4.3. Bolometric magnitudes

The bolometric correction $BC_K = M_{\mathrm{bol}} - M_K$, obtained from the total luminosity and the K_s-band magnitude (corrected for extinction and distance modulus) is shown in Fig. 5 as a function of $J - K_s$ colour. To extend our data points to redder colours, we included also LMC and SMC data from Groenewegen et al.
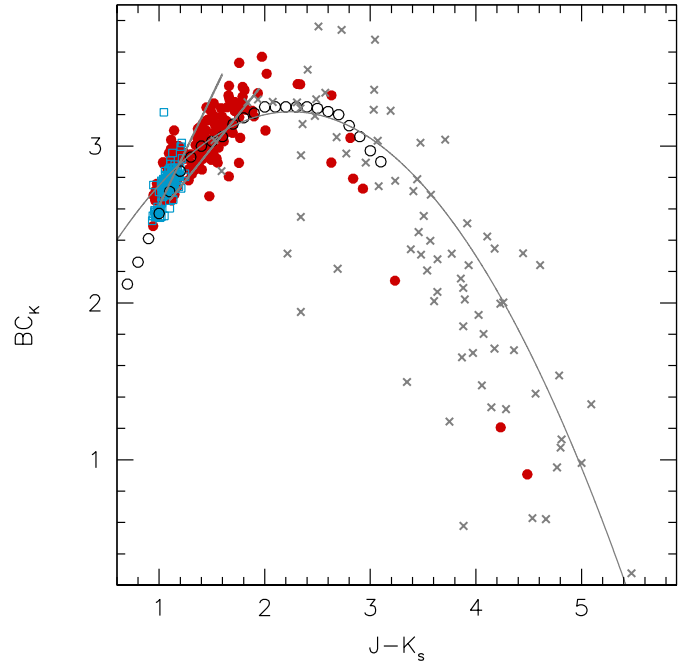

Fig. 5: Bolometric correction as a function of near-IR colour. O-rich stars are shown as *blue open squares* and C-rich stars as *filled red circles*. *Crosses* are data for C-stars in the LMC and SMC from Groenewegen et al. (2009). The open black circles show the relation for Galactic C-stars from Bergeat et al. (2002), the lines are taken from Kerschbaum et al. (2010); the curved line is for C-stars, while the two straight lines define the region of O-rich stars.

(2009). Our data are fully consistent with other literature data (Bergeat et al. 2002; Kerschbaum et al. 2010). The only (possi-
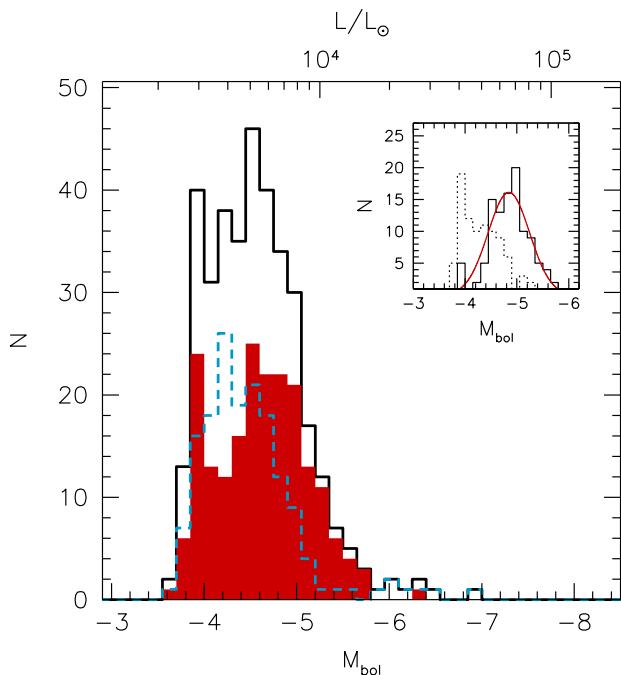
Fig. 6: Bolometric luminosity function of AGB stars. The *filled histogram* and the *dashed line* show the LF obtained from C-rich and O-rich stars, respectively. The inner panel shows the LF for dust-free (*dotted*) and dusty (*solid*) AGB C-stars. The solid curve is a Gaussian fit to the histogram of dusty stars.
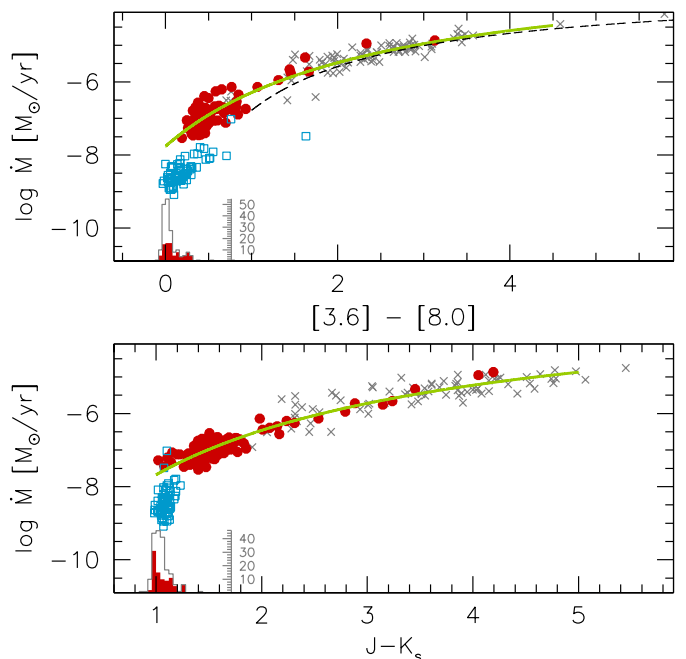

Fig. 7: Mass-loss rates as a function of IR colours. Symbols are the same as in Fig. 5. The grey open histogram shows the colour distribution of dust-free AGB stars; the red histogram is the distribution of C-stars alone. The solid line is the best fit to all C-stars, including the Groenewegen et al. (2009) data. The dashed line in the upper panel is the relation of Matsuura et al. (2009).

ble) exception could be represented by the extremely red C-stars at $J - K_s \gtrsim 2.5$ mag. For these stars the BCs obtained from both our data and those of Groenewegen et al. (2009) are located 0.3 mag below the Kerschbaum et al. (2010) relation. Note however that this relation is not well defined at $J - K_s > 2.5$ mag, since the sample of Kerschbaum et al. (2010) contains only few red stars, which exhibit a significant scatter and lie – on average – below the best-fitting relation. We can therefore conclude that the bolometric magnitudes obtained from the SED fits are in agreement with literature data at a level of – at worst – few tenths of magnitude.

The bolometric LF function obtained for all AGB stars in our sample is shown in Fig. 6. The cut at the faint end, around $M_{bol} = -3.7$ mag, is the consequence of the selection cut for stars fainter than the TRGB. The overall LF peaks at $M_{bol} = -4.5$ mag and drops at magnitudes brighter than $M_{bol} \sim -5.0$ mag. There are very few stars brighter than $M_{bol} = -6.0$ and none above the classical limit for AGB stars, $M_{bol} = -7.1$ (Paczyński 1971), corresponding to a Chandrasekhar-limit core-mass before core He ignition. The most massive AGB stars, undergoing "hot bottom burning", may have a luminosity brighter than the classical AGB limit (see, e.g., Groenewegen et al. 2009; García-Hernández et al. 2009), but their number is expected to be extremely small.

The LF of C-rich stars shows a bimodality, which can be understood by considering separately the LFs for stars whose best-fitting solution is dust-free and and stars with dusty envelopes. Dust-free stars show a decreasing LF, truncated by the selection cut. Dusty C-stars are typically brighter – as already noted by van Loon et al. (1999) – and their LF is well described by a Gaussian function centred at $M_{bol} = -4.84$ mag and with $\sigma = 0.40$ mag. The peak of the LF is in perfect agreement with other observations of LMC C-stars and fully con-

sistent with the expectations of theoretical models (see, e.g., Groenewegen & de Jong 1993). Some of the faintest AGB stars classified as C-rich could actually be misclassified O-rich stars, since our classification procedure is less precise for faint and blue stars, but in any case, our result seems to indicate the presence of a non negligible population of AGB stars fainter than the TRGB characterised by very low – if any – mass-loss rates. This is in agreement with the prediction of recent evolutionary models, in contrast with the paucity of faint C stars in spectroscopic surveys (Kontizas et al. 2001; Gullieuszik et al. 2008; Marigo et al. 2008). We will reserve a more detailed discussion of this issue for a future paper, presenting a comparison of our data with the predictions of theoretical evolutionary models.

Recently, Srinivasan et al. (2011) presented a C-star LF, revising their earlier work (Srinivasan et al. 2009). The general shape and the position of the peak in the revised LF is in good agreement with our result.

4.4. Mass-loss rates

Figure 7 shows mass-loss rates as a function of IR colours. The data points lie on a well defined sequence, fully compatible with data published in Groenewegen et al. (2009), showing that our fitting technique, based only on photometric observations, provides reliable mass-loss rates. Also in this case, the main limitation of our results is due to the poor statistics for the reddest dusty stars. We have no O-rich stars with noticeable mass-loss. The number of dusty C-stars is still very small, but the sequence of the few data points redder than $J - K_s \sim 2$ mag exhibits a remarkably low dispersion. From a least-squares fit to all data,

including those of Groenewegen et al. (2009), we obtained the following relation for C-stars:

$$\log \dot{M} = \frac{-15.42}{(J - K_s) + 2.10} - 2.70 \qquad (2)$$

for $1.0 < J - K_s < 5.0$ mag; and

$$\log \dot{M} = \frac{-12.78}{([3.6] - [8.0]) + 2.49} - 2.63 \qquad (3)$$

for $0.0 < [3.6] - [8.0] < 4.5$ mag. For the bluest stars in our sample the mass-loss rates are extremely low, at the detection limit of our method. At $J - K_s \sim 1.0$ mag, the best-fitting model was dust-free for most stars; for the others, the mass-loss rates are less than $\sim 10^{-7} M_\odot \, \mathrm{yr}^{-1}$. A conservative approach would suggest that the measured values for the bluest stars must therefore be considered upper limits. The blue applicability limits of Eqs. (2) and (3) were based on this consideration and on the colour distributions for dust-free stars in Fig. 7. On the other hand, the definition of the red limit is somewhat arbitrary and it was set by the colour of the reddest stars in our sample. The upper panel of Fig. 7 compares our results with the relation of Matsuura et al. (2009), obtained using all measures of Groenewegen et al. (2009). The difference for stars bluer than [3.6]-[8.0]= 2 mag is mainly due to the small number of stars in this colour range in the Groenewegen et al. (2009) sample. The relation of Matsuura et al. (2009) is therefore weakly constrained for the bluest stars. In addition, their relation is derived using the colours obtained from the best-fitting SEDs, rather than the observed counterparts, as in our case. The difference is therefore related to the systematic offsets already discussed in Sect. 3. We conclude that our relation is more reliable when mass-loss rates are estimated from observed photometry.

5. Discussion and Conclusion

In this paper we used the first data from the ESO public survey VMC to obtain optical to mid-IR SEDs for a sample of 367 AGB stars candidates. Our selection criteria were defined to minimise the selection bias. Sources with colours as blue as the RGB and fainter than $K_s = 12.0$ mag –which roughly corresponds to the tip of the RGB in the LMC– were excluded since this region of the CMD is dominated by the RGB and it is nearly impossible to disentangle RGB and AGB stellar populations from photometric data.

Luminosities and mass-loss rates were obtained by fitting the SEDs with a dust radiative transfer model. Mass-loss rates were obtained assuming a constant expansion velocity and dust-to-gas ratio with values similar to Galactic AGB stars.

The cumulative distribution of mass-loss rates for O- and C-rich stars is shown in Fig. 8. The total mass-loss rate in the 1.42 deg^2 area encompassed by our analysis is $6.4 \times 10^{-5} \, M_\odot \, \mathrm{yr}^{-1}$. This value is lower than that expected from the average mass-loss rate for the external regions of the LMC found by Matsuura et al. (2009), which is $1.1 \times 10^{-4} \, M_\odot \, \mathrm{yr}^{-1}$ – scaled to a 1.42 deg^2 area. We note however that the ERO object discussed in the Appendix was excluded from our analysis. Matsuura et al. (2009) considered it to be an AGB and estimated for it $\dot{M} = 6.4 \times 10^{-5} \, M_\odot \, \mathrm{yr}^{-1}$. This object alone could explain the difference between the integrated mass-loss rates.

Table 5 shows the star counts and the integrated mass-loss rates for stars in different mass-loss ranges, together with the star counts for the external region of the LMC from Matsuura et al.
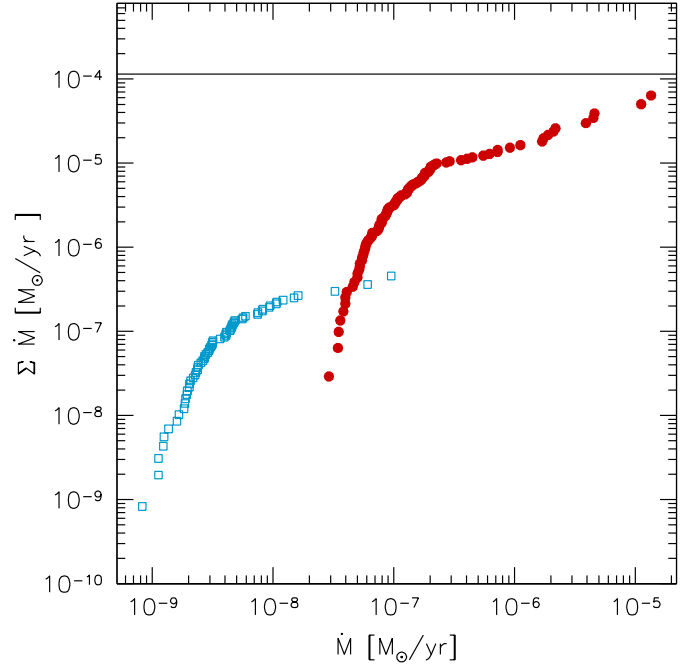

Fig. 8: Cumulative distribution of the mass-loss rates for O- (*open squares*) and C-rich (*filled dots*) AGB stars. The horizontal line shows the average mass-loss rates of the external regions of the LMC obtained by Matsuura et al. (2009), rescaled to the area encompassed by our analysis.

Table 5: Distribution of mass-losing O- and C-rich stars. The second column shows the star counts of Matsuura et al. (2009) for C-stars in the external region of the LMC rescaled to the area encompassed by our analysis. The last two columns are the star counts and total mass-loss rates obtained from this study.

$\dot{M}$ range $M_\odot \, \mathrm{yr}^{-1}$	C-rich N_{M09}	N	$\dot{M}_{TOT}$ $10^{-5} M_\odot \, \mathrm{yr}^{-1}$
$< 1 \times 10^{-6}$	9.1	102	1.5
$1 \times 10^{-6} < \dot{M} < 3 \times 10^{-6}$	8.1	6	1.1
$3 \times 10^{-6} < \dot{M} < 6 \times 10^{-6}$	4.4	3	1.3
$6 \times 10^{-6} < \dot{M} < 1 \times 10^{-5}$	1.8	0	0
$1 \times 10^{-5} < \dot{M} < 3 \times 10^{-5}$	1.8	2	2.5
$3 \times 10^{-5} < \dot{M} < 6 \times 10^{-5}$	0.5	0	0
$> 6 \times 10^{-5}$	0.2	0	0
Total:			6.4
$\dot{M}$ range	O-rich N_{M09}	N	$\dot{M}_{TOT}$
$< 1 \times 10^{-6}$	-	65	0.05
Total:			0.05

(2009). Since Matsuura et al. (2009) considered only C-stars, O-rich stars are not taken into account in Table 5. The star counts are in good agreement, and the only significant discrepancy is related to stars with low mass-loss rates. This is due to the selection criteria adopted by Matsuura et al. (2009), biased towards red stars. The 102 stars with $\dot{M} < 10^{-6} \, M_\odot \, \mathrm{yr}^{-1}$ contribute to $\sim 24\%$ of the total mass-loss rate, and the two stars with higher mass-loss rates contribute up to 38 % of the total. The fact that the inte-

grated mass-loss rate is strongly dominated by the most extreme stars, prevents us from drawing any conclusion on the overall mass-loss rate in the LMC from the relatively small number of stars in our sample. The highest values of the mass-loss rates in the LMC can be as high as $\sim 10^{-4}\,M_\odot\,\mathrm{yr}^{-1}$ (e.g., Gruendl et al. 2008). To reach a more robust estimate we therefore need to extend our analysis to a much larger area. The 65 mass-losing O-rich stars have an integrated mass-loss rate of $4.5 \times 10^{-7}\,M_\odot\,\mathrm{yr}^{-1}$, which is negligible compared to the C-stars. Nevertheless, this is not true in general, since extreme O-rich AGB stars can have mass-loss rates as high as the integrated value of our sample (van Loon et al. 2005; Groenewegen et al. 2009).

The main limitations of the results reported in this paper are related to the relatively small number of dust-enshrouded AGB stars in our sample. The main aim of our work was to explore the confidence level of the mass-loss rates and bolometric magnitude measures derived from photometric SEDs constructed by combining VMC data with optical MCPS, near-IR 2MASS and mid-IR Spitzer data, with a view to applying our method to the complete sample of AGB stars that will be observed by VMC in the Magellanic system. We demonstrated the reliability of the measures and classification of the O- and C-rich AGB stellar populations. A more complete picture about the mass-loss return and the process of enrichment of the ISM will be obtained from forthcoming VMC observations. VMC is scheduled to regularly carry out observations which, at the end of the 5 year survey, will provide photometry for two orders of magnitude more AGB stars. Our results are nevertheless important, because our database already contains a sufficiently large number of stars with colours up to $J - K_s \simeq 2$ mag, which represent the bulk of the AGB population.

References

Aringer, B., Girardi, L., Nowotny, W., Marigo, P., & Lederer, M. T. 2009, A&A, 503, 913

Battinelli, P. & Demers, S. 2005, A&A, 434, 657

Bergeat, J., Knapik, A., & Rutily, B. 2002, A&A, 390, 967

Bolatto, A. D., Simon, J. D., Stanimirović, S., et al. 2007, ApJ, 655, 212

Buchanan, C. L., Kastner, J. H., Hrivnak, B. J., & Sahai, R. 2009, AJ, 138, 1597

Cardelli, J. A., Clayton, G. C., & Mathis, J. S. 1989, ApJ, 345, 245

Cioni, M., Clementini, G., Girardi, L., et al. 2011, A&A, 527, A116

Cioni, M., Girardi, L., Marigo, P., & Habing, H. J. 2006, A&A, 448, 77

Cioni, M.-R. L., van der Marel, R. P., Loup, C., & Habing, H. J. 2000, A&A, 359, 601

Cordier, D., Pietrinferni, A., Cassisi, S., & Salaris, M. 2007, AJ, 133, 468

Emerson, J. & Sutherland, W. 2010, The Messenger, 139, 2

Emerson, J. P., Irwin, M. J., Lewis, J., et al. 2004, in eds, Proc. SPIE, Vol. 5493, Optimizing Scientific Return for Astronomy through Information Technologies, Bellingham, ed. P. J. Quinn & A. Bridger, 401

García-Hernández, D. A., Manchado, A., Lambert, D. L., et al. 2009, ApJ, 705, L31

Girardi, L., Williams, B. F., Gilbert, K. M., et al. 2010, ApJ, 724, 1030

Gordon, K. D., Meixner, M., Meade, M. R., et al. 2011, AJ, 142, 102

Groenewegen, M. A. T. & de Jong, T. 1993, A&A, 267, 410

Groenewegen, M. A. T., Sloan, G. C., Soszyński, I., & Petersen, E. A. 2009, A&A, 506, 1277

Groenewegen, M. A. T., Whitelock, P. A., Smith, C. H., & Kerschbaum, F. 1998, MNRAS, 293, 18

Gruendl, R. A. & Chu, Y.-H. 2009, ApJS, 184, 172

Gruendl, R. A., Chu, Y.-H., Seale, J. P., et al. 2008, ApJ, 688, L9

Gullieuszik, M., Held, E. V., Rizzi, L., et al. 2008, MNRAS, 388, 1185

Gustafsson, B., Edvardsson, B., Eriksson, K., et al. 2008, A&A, 486, 951

Hambly, N. C., Mann, R. G., Bond, I., et al. 2004, in eds, Proc. SPIE, Vol. 5493, Optimizing Scientific Return for Astronomy through Information Technologies, Bellingham, ed. P. J. Quinn & A. Bridger, 423

Held, E. V., Gullieuszik, M., Rizzi, L., et al. 2010, MNRAS, 404, 1475

Irwin, M. J., Lewis, J., Hodgkin, S., et al. 2004, in eds, Proc. SPIE, Vol. 5493, Optimizing Scientific Return for Astronomy through Information Technologies, Bellingham, ed. P. J. Quinn & A. Bridger, 411

Ishihara, D., Onaka, T., Kataza, H., et al. 2010, A&A, 514, A1

Ita, Y., Onaka, T., Kato, D., et al. 2008, PASJ, 60, 435

Ivezić, Z., Nenkova, M., & Elitzur, M. 1999, arXiv:astro-ph/9910475

Kato, D., Nagashima, C., Nagayama, T., et al. 2007, PASJ, 59, 615

Kemper, F., Woods, P. M., Antoniou, V., et al. 2010, PASP, 122, 683

Kerschbaum, F., Lebzelter, T., & Mekul, L. 2010, A&A, 524, A87

Kontizas, E., Dapergolas, A., Morgan, D. H., & Kontizas, M. 2001, A&A, 369, 932

Lagadec, E., Verhoelst, T., Mékarnia, D., et al. 2011, MNRAS, 1426

Marigo, P. 2002, A&A, 387, 507

Marigo, P., Girardi, L., Bressan, A., et al. 2008, A&A, 482, 883

Matsuura, M., Barlow, M. J., Zijlstra, A. A., et al. 2009, MNRAS, 396, 918

Meixner, M., Gordon, K. D., Indebetouw, R., et al. 2006, AJ, 132, 2268

Miszalski, B., Napiwotzki, R., Cioni, M.-R. L., et al. 2011, A&A, 531, A157

Paczyński, B. 1971, Acta Astron., 21, 417

Renzini, A. & Buzzoni, A. 1986, in Astrophysics and Space Science Library, Vol. 122, Spectral Evolution of Galaxies, ed. C. Chiosi & A. Renzini, 195

Renzini, A. & Voli, M. 1981, A&A, 94, 175

Rubele et al. 2011, A&A, submitted

Sargent, B. A., Srinivasan, S., & Meixner, M. 2011, ApJ, 728, 93

Schaefer, B. E. 2008, AJ, 135, 112

Schlegel, D. J., Finkbeiner, D. P., & Davis, M. 1998, ApJ, 500, 525

Skrutskie, M. F., Cutri, R. M., Stiening, R., et al. 2006, AJ, 131, 1163

Sloan, G. C., Kraemer, K. E., & Bernard-Salas, J. 2010, in Bulletin of the American Astronomical Society, Vol. 42, American Astronomical Society Meeting Abstracts #215, 459,02

Srinivasan, S., Meixner, M., Leitherer, C., et al. 2009, AJ, 137, 4810

Srinivasan, S., Sargent, B. A., & Meixner, M. 2011, A&A, 532, A54+

van der Veen, W. E. C. J., Habing, H. J., & Geballe, T. R. 1989, A&A, 226, 108

van Loon, J. T., Cioni, M.-R. L., Zijlstra, A. A., & Loup, C. 2005, A&A, 438, 273

van Loon, J. T., Cohen, M., Oliveira, J. M., et al. 2008, A&A, 487, 1055

van Loon, J. T., Groenewegen, M. A. T., de Koter, A., et al. 1999, A&A, 351, 559

Véron-Cetty, M.-P. & Véron, P. 2010, A&A, 518, A10

Volk, K. & Kwok, S. 1988, ApJ, 331, 435

Woods, P. M., Oliveira, J. M., Kemper, F., et al. 2011, MNRAS, 411, 1597

Zaritsky, D., Harris, J., Thompson, I. B., & Grebel, E. K. 2004, AJ, 128, 1606

Zaritsky, D., Harris, J., Thompson, I. B., Grebel, E. K., & Massey, P. 2002, AJ, 123, 855

Appendix A: J050343.02-664456.7

This section is dedicated to a more detailed analysis of the extremely red source J050343.02-664456.7. It is one of the reddest sources in our sample, and one of two objects detected only in the mid-IR, with no counterpart in the VMC catalogue – the other one being a YSO.

J050343.02–664456.7 is one of the 13 sources identified by Gruendl & Chu (2009) and generically classified –on the basis of their photometric SED– as EROs. Subsequent Spitzer/IRS spectroscopic observations of seven of them revealed that they are extreme carbon stars (Gruendl et al. 2008). The conclusion is based on the detection of SiC and C_2H_2 absorption and on the presence of a broad MgS feature in two cases.

Assuming that these objects are AGB stars, the derived mass-loss rates are higher than those of any known carbon-rich AGB star in the LMC. Gruendl et al. (2008) estimated a mass-loss rate $\dot{M} = 1.5 \times 10^{-4}\,M_\odot\,\mathrm{yr}^{-1}$ for J050343.02–664456.7. From empirical relations based on mid-IR colours, Matsuura et al. (2009) found a lower value, viz. $6.4 \times 10^{-5}\,M_\odot\,\mathrm{yr}^{-1}$. This object alone provides a contribution equal –or bigger– than the integrated
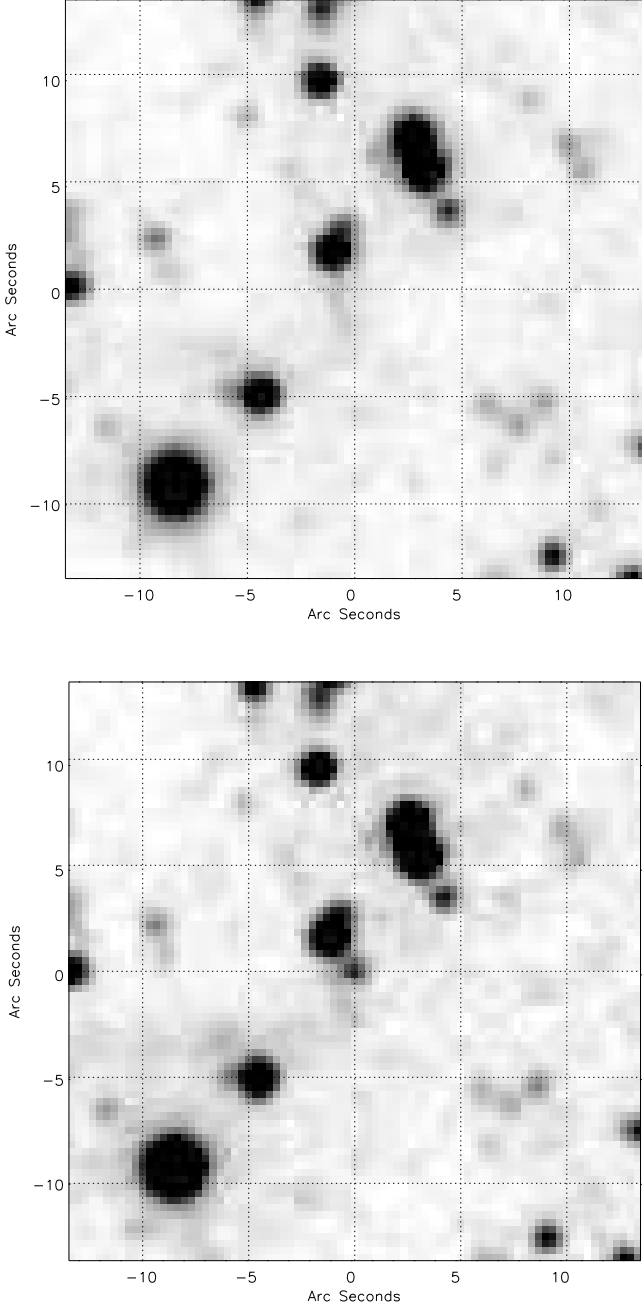
Fig. A.1: $30'' \times 30''$ J (*upper panel*) and K_s (*lower panel*) VMC images centred on the Extremely Red Object J050343.02-664456.

Fig. A.2: Photometric data points and standard AGB SED model for the Extremely Red Objects J050343.02-664456 (*diamonds and solid line*). In the upper panel they are compared with data and SED standard model for J055026.08-695603.1 (*(circles and dotted line*). The lower panel show the post-AGB model with a detached dusty shell *(dotted line)*. The arrows show the photometric detection limits.

mass-loss rate of all stars in our sample. In the following we present some indications that J050343.02–664456.7 may not be a *normal* AGB star.

J050343.02–664456.7 is not present in the VMC catalogue because it is detected only in the K_s-band. It is in fact completely invisible in the J band as well as in the bluer Y band, as shown in Fig. A.1. The vmcSource catalogue is built with sources detected in the three VMC bands (Cioni et al. 2011) and therefore J050343.02-664456.7 is not included. The K_s magnitude was obtained from the vmcDetection table, i.e. the catalogue corresponding to individual observations. Its value is $K_s = 18.75$ mag.
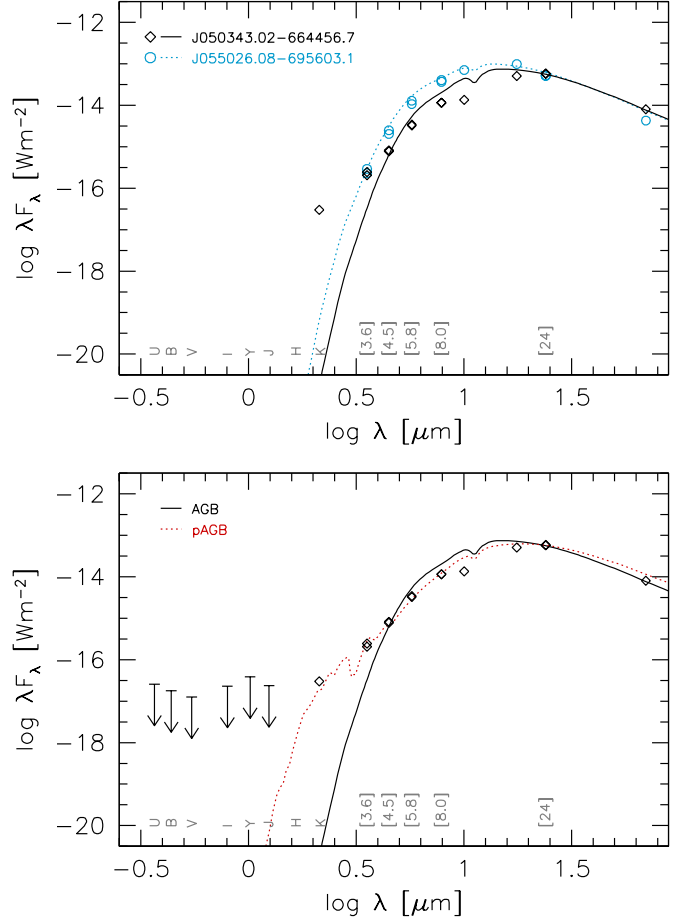
The photometric data points and the best-fitting model of J050343.02-664456.7 obtained using the standard procedure described in Sect. 3 are presented in Fig. A.2. The model substantially underestimates the flux in the bluest part of the SED, in the K_s and in the IRAC 3.6 μm bands. The predicted K_s magnitude is ~ 9 mag fainter than the observed one. We tested our model also on the other EROs identified by Gruendl & Chu (2009) –all located outside the 8_3 VMC tile and hence not included in our sample– and found that in most cases our AGB models could describe quite well the observed SED. As an example, in Fig. A.2 we show the photometric data and our best-fitting SED model for J055026.08695603.1, an EROs with a SED similar to the one of J050343.02-664456.7. In this case the model SED seems to generally better reproduce the observed data. We are therefore led to consider the possibility that J050343.02-664456.7 could be something different from an AGB star.

The SED of J050343.02-664456.7 could be explained assuming that this is a post-AGB star with a detached shell. In this case the flux in the near-IR would be due to the contribution of the central star. In our case this contribution is extremely low, and produces only a flatter SED in the near-IR, rather than a secondary peak in the near-IR (see, e.g., Lagadec et al. 2011). This

implies that the central star stopped losing mass –i.e. it ended the AGB phase– very recently (see, e.g., van der Veen et al. 1989).

To explore the post-AGB hypothesis, we used our models setting the condensation temperature of the dust grains as a free parameter. The resulting best-fitting model is shown in the lower panel of Fig. A.2 as a dotted line. It is compatible with the upper limit for optical and near-IR magnitudes corresponding to the MCPS and VMC detection limit and it shows a much better agreement with the observed SED than the standard AGB model. In the best-fitting model the condensation temperature is $T_c = 330$ K, corresponding to an inner radius of the dusty shell of $\sim 5 \times 10^4 R_\odot$ or $\sim 3.5 \times 10^{10}$ km. This value is extremely small, just 10 times bigger than the inner radius of the dusty shell obtained for the standard model. This implies that the mass-loss production in J050343.02-664456.7 has dropped to zero extremely recently –of the order of ~ 100 years ago assuming a shell expansion velocity of 10 km s^{-1}.

To conclude, we showed that the observed SED of J050343.02-664456.7 is not fully compatible with a standard model for AGB stars, showing a flux excess at wavelengths shorter than ~ 4 μm. We proposed that this source could belong to the –rare– class of objects in transition from the AGB to the planetary nebula stage. Further evidence supporting this idea could be found in the fact that some of the SEDs of the 13 EROs identified by Gruendl & Chu (2009) show hints of a secondary peak at near-IR wavelengths. We hence point out that it may be not so straightforward to classify all EROs as AGB carbon stars.